Stopping of energetic cobalt clusters and formation of radiation damage in graphite

Stopping of energetic cobalt clusters and formation of radiation damage in graphite

Vladimir N. Popok* and Saša Vučković
Department of Physics, University of Gothenburg, 41296 Gothenburg, Sweden

Juha Samela, Tommi T. Järvi, and Kai Nordlund
Department of Physics, University of Helsinki, P.O. Box 43, Helsinki FI-00014, Finland

Eleanor E. B. Campbell
School of Chemistry, Edinburgh University, West Mains Road, Edinburgh, EH9 3JJ Scotland, United Kingdom and Division of Quantum Phases and Devices, School of Physics, Konkuk University, Seoul 143-701, Korea
(Received 4 August 2009; revised manuscript received 14 October 2009; published 19 November 2009)

The interaction of energetic (up to 200 eV/atom) size-selected Co_n clusters with HOPG is studied both experimentally and theoretically. Etching of the radiation damaged areas introduced by cluster impacts provides a measure of the depth to which the collision cascades are developed and allows a comparison of these data with the molecular dynamics simulations. Good agreement between the experimental results and modeling is obtained. It is shown that the projected range of the cluster constituents can be linearly scaled with the projected momentum (the cluster momentum divided by surface impact area). With decrease in cluster energies to ca. 10 eV/atom the transition from implantation to pinning is suggested. It is found that even after quite energetic impacts residual clusters remain intact in the shallow graphite layer. These clusters can catalyze reaction of atmospheric oxygen with damaged graphite areas under the thermal heating that leads to the formation of narrow (5–15 nm) random in shape surface channels (trenches) in the top few graphene layers. Thus, small imbedded Co nanoparticles can be used as a processing tool for graphene.

DOI: 10.1103/PhysRevB.80.205419 PACS number(s): 61.80.Jh, 81.05.Uw, 83.10.Rs, 81.65.Cf

I. INTRODUCTION

Atomic and molecular clusters of various species with sizes in the nanometer scale are subjects of intensive study. They can be used as models for investigation of fundamental physical aspects of the transition from atomic scale to bulk material, as building blocks for nanodevices, and as controllable and versatile tools for modification of surfaces and shallow layers.[1–4]

Practical applications of cluster beams require a good knowledge of the physics behind interactions of atomic agglomerates with material. There are a number of specific phenomena assigned to energetic clusters impinging on substrates.[3] For instance, the overlap of collision cascades produced by individual cluster constituents causes much higher radiation damage compared to the conventional atomic ion implantation. The interaction is also characterized by a high degree of nonlinearity,[5] which arises from the fact that the cluster atoms influence each other during penetration into the target and locally transfer a high-energy density to the substrate. On the other hand, a violent interaction of a cluster with a few surface layers of the target can lead to extensive mixing of cluster constituents with substrate atoms that favors doping of very shallow layers for applications in electronics.[4,6] Recently, this direction has been developed into a new in-fusion technique.[6] The effect of the high density of the energy transferred from the cluster at the beginning of the impact can be compared with a nanoscopic analog of a meteorite-planet collision that typically results in crater formation.[7–9] Thus, high-fluence energetic cluster beams can be used for very efficient sputtering of surfaces as well as for smoothing.[4] For successful practical applications of energetic cluster beams, a theory of cluster stopping in matter is required. However, such a theory is still under development, even though cluster-solid interactions have been studied for the past 10–15 years. In particular, the different simulations and experiments of cluster implantation show rather different scaling laws for the projected ranges of cluster constituents and the depth of radiation damage.[3,10]

Quantum size effects that influence the electronic, optical and magnetic properties make arrays of nanoparticles or nanoparticulate materials very attractive for nanotechnology. However, control of nanoparticle or cluster size becomes an important issue. It is well known that soft landing of clusters often leads to their diffusion followed by coagulation or agglomeration, ruining the advantages of size selection.[11] One possibility to immobilize the deposited clusters, i.e., preserve their size, is to gently increase the deposition energy in order to approach the so-called pinning regime where defects, created in the surface layer on impact, serve as binding sites for the cluster.[12] The possibility of pinning has been shown for different cluster species on graphite.[13,14]

Graphite is often chosen for surface experiments because it is a good model material, it has an atomically smooth surface that makes it easy to resolve very small deposited clusters or radiation damaged areas, and post-implantation thermal treatment gives a possibility to extract the depth of the introduced radiation damage (this procedure is discussed in more detail in the next section). Among metal nanoparticles or clusters, cobalt attracts considerable attention because of its interesting electronic and magnetic properties that are promising for applications in spintronics.[15] Cobalt nanoparticles also have well-known catalytic properties, for instance, to grow carbon nanotubes[16] or can be used for the processing and cutting of graphene layers.[17] The determination of the pinning threshold for cobalt clusters is of consid-

erable importance for preparation of surfaces with size-selected nanoparticles that can be used in catalysis, detection of gas pollutants and spintronics.

In this paper, we present experimental results and molecular dynamics (MD) simulations on implantation and deposition of size-selected Co_n clusters in/on highly ordered pyrolytic graphite (HOPG). MD has become a widely used method with the development of computer techniques. This method is especially suitable for simulations of dynamics of large groups of interacting atoms and, therefore, it has been used for impact modeling.[18] We present a detailed discussion of the change in the cluster-surface interaction mechanism from implantation to pinning with decreasing cluster kinetic energy and momentum. Then we present a model of cluster stopping, in which the projected ranges of cluster constituents and the depth of radiation damage scale linearly with cluster momentum per impact area. Finally, we demonstrate and explain an effect of catalytically enhanced (by pinned Co_n clusters) selective surface etching of graphite.

II. EXPERIMENTAL METHODS

Clusters of cobalt were produced using a laser ablation cluster source (LACS). The second harmonic (532 nm) of a Nd:YAG laser was utilized for the material vaporization. Constructional and operational details of the source are described elsewhere.[19] The source was attached to a cluster implantation and deposition apparatus (CIDA).[20,21] This combination provides the possibility to produce metal clusters and manipulate the cluster beam, in particular, to separate the cationic clusters from neutral and anionic ones, control their size and kinetic energy (velocity) and carry out deposition and implantation experiments under ultrahigh-vacuum (UHV) conditions.[19,22] A time-of-flight mass spectrometer in the Wiley-McLaren configuration together with a multichannel plate detector is used to obtain the mass spectra of cluster ions. The detection efficiency decreases with decreasing impact velocity, i.e., increasing cluster mass. By having relatively high-cluster velocities (acceleration potentials up to 4 kV) we were able to detect and resolve Co_n^+ cluster ions with n over 200. However, for the current series of experiments, the cluster ions were accelerated with voltages up to only 1.5 kV at the initial stage to ensure the required size selection. This explains the resolution of clusters with n up to only ca. 80 atoms in the mass spectrum presented in Fig. 1. For impact experiments reported here with energies higher than 1.5 keV, the clusters were additionally accelerated after the size selection.

Size-selected Co_n^+ cluster ions ($n=30\pm4$, 50 ± 5 and 63 ± 5) with mean energies E between 0.25 and 10.1 keV/cluster ($E_{at}=5-200$ eV/atom) were used for deposition and implantation experiments (see Table I for details). The deposition/implantation was carried out on/in HOPG of ZYB quality (purchased from NT-MDT). Surfaces of the HOPG samples were cleaved with the help of an adhesive tape before placement in the load-lock vacuum chamber, which was then quickly evacuated to a vacuum of 10^{-7} Torr. After that, the sample was moved into the implantation chamber at a pressure of $(1-2)\times10^{-9}$ Torr and exposed to the cluster beam.

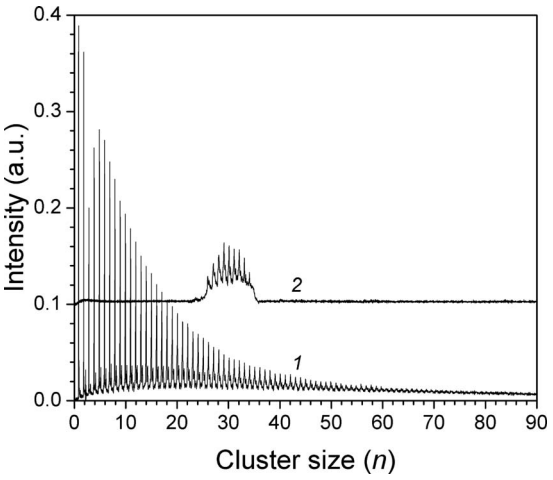

FIG. 1. Mass spectra of Co_n clusters (1) before and (2) after size selection of $Co_{30\pm4}$.

Surfaces of the implanted samples were studied *ex situ* using a scanning probe microscope from NT-MDT. Scanning tunneling microscopy (STM) measurements were carried out in the constant current mode with a bias of 70–100 mV using PtIr tips. After the initial STM study the samples were heated at 600 °C for 3 min. in a furnace in ambient atmosphere. It

TABLE I. Mean diameters and heights of bumps observed by STM on HOPG after implantation of Co_n clusters with various energies.

Mean cluster size (n)	Mean E_{at} (eV)	d (nm)	h (Å)
Co_{30}	9	1.3	3.0
	13	1.5	2.8
	53	2.4	3.2
	100	3.5	3.6
	150	4.3	3.5
	200	4.5	4.0
Co_{50}	5	1.4	3.0
	6	1.4	3.0
	7	1.4	3.3
	9	1.4	3.2
	12	1.6	3.7
	20	2.0	3.3
	30	2.2	3.5
	60	2.5	4.0
	97	3.3	3.2
	150	3.7	4.4
	200	4.4	4.2
Co_{63}	7	1.8	3.0
	13	2.6	3.7
	50	2.8	3.7
	100	3.5	4.2
	130	4.0	3.8
	160	4.1	4.0

is known that heating of pristine graphite above ca. 500 °C can lead to the formation of pits of circular or hexagonal shape with depths of 1–2 graphite planes or monolayers (MLs). This is due to the presence of surface defects promoting chemical reactions of carbon with oxygen.[23,24] The pit diameter depends on the etching time. It was shown elsewhere that monomer or cluster ion implantation followed by heat treatment in the presence of oxygen leads to the formation of pits with the depth corresponding to the depth of the radiation damage cascades developed by the projectiles.[25] Etching removes only the damaged volume and it does not attack the underlying graphite planes. Hence, one can experimentally and quite precisely measure the depth of the radiation damage for the implanted graphite samples. Therefore, the heated (etched) samples were studied again by STM and additionally by atomic force microscopy (AFM) in tapping mode using ultrasharp cantilevers with diamond-like carbon tips (curvature radius of 1–3 nm).

III. COMPUTER SIMULATIONS

Cluster ion impacts were simulated with classical MD. The main principles of the molecular dynamics algorithms are presented in Refs. 26 and 27. The adaptive time step and electronic stopping algorithms are the same as in Ref. 18. The interaction between Co atoms was described with an embedded-atom-method (EAM) potential[28] and the Co_n clusters were relaxed using this potential before the impact simulations. The graphite structure was modeled using an improved Tersoff potential,[29] which includes a Lennard-Jones type interaction between graphite layers. A Morse pair potential was used for C-Co interactions. It is discussed later in this section. A short-range repulsive force[30] was also present between all pairs of atoms to better describe collisions of atoms. Electronic stopping was applied to all atoms that had kinetic energies higher than 5 eV. Test simulations show that the strength and threshold for the electronic stopping effect[31] does not significantly influence the results in this case.

In the simulations, a graphite surface was bombarded at normal incident angle with Co_n clusters, $n=30$, 50, 63, 100, and 200. Both orientation of the impacting cluster and the impact point were randomly varied. At these cluster sizes, the forms and depths of damaged regions do not vary much between simulations, so only a few randomly varied cases are needed to get reliable averages of cluster ranges. The size of the graphite surface was 19×18 nm and the thickness of 5.4 nm. The borders of the graphite were cooled to prevent waves induced by the impact to return back to the impact region over periodic boundaries. Simulation times were 5–20 ps depending on the impact energy. Test simulations with longer times showed that the damaged area does not change after that at the energies used in the simulations (1–200 eV/atom).

The Morse potential used to describe the C-Co interactions has two parameters, the equilibrium bond distance r_0 and the corresponding potential energy E_0. In the cobalt carbide dimer, CoC, $r_0=1.56$ Å, and $E_0=1.8$ eV/atom.[32] However, these values cannot be used as pair potential parameters because the strong cobalt carbide bonding gives unphysical results in Co_n cluster impact simulations where Co atoms can interact with several C atoms simultaneously. Instead, $r_0=2.0$ Å is a reasonable choice for the equilibrium distance because in larger structures than the CoC molecule, experimental Co-C bond lengths are between 1.94–2.15 Å.[33–35] If we assume that a Co atom on graphene interacts with six C atoms, we can approximate that $E_0=0.3$ eV/atom. This value is used in the simulations because it gives cluster ranges that are in agreement with experimental ones. The change to E_0 in the range from 0.1 to 0.5 eV affects the impact energy threshold of the Co penetration through the first graphite layer. However, the scaling behavior of cluster range extracted from the simulations is not particularly sensitive to changes of equilibrium energy within the tested energy range, although the absolute values of cluster ranges vary with E_0.

TABLE II. Properties of dimers calculated with PBE-DFT and reference values.

Dimer	Reference	Multiplicity	Energy (eV/atom)	r (Å)
C_2	This work	3	3.47	1.31
	46	1	3.20	1.24
Co_2	This work	5	1.46	1.96
	46,51		<0.66	
	49		1.7	
CoC	This work	2	2.51	1.55
	34	2	1.9	1.56

To get deeper insight into the binding between cobalt and the graphite surface, density functional theory (DFT) calculations were used. The Vienna *ab initio* simulation package (VASP) (Refs. 36–39) was used for this purpose with the plane-augmented-wave method and pseudopotentials[40,41] in the Perdew-Burke-Ernzerhof (PBE) generalized gradient approximation.[42] All calculations were spin polarized, with an energy cutoff of 520 eV and for the partial occupancies, we used the tetrahedron method with Blöchl corrections.[43] For calculations involving a graphite surface, Monkhorst-Pack k-point sampling of $4\times4\times1$ was used, whereas only the Gamma point was used for dimers and atoms in vacuum. In stated energies, the energies of C and Co atoms in vacuum, −1.37 and −1.99 eV, respectively, have been taken into account.

For reference, the nearest neighbor C-C distance and the cohesive energy of a single graphene sheet were calculated with DFT. For graphite, a nearest-neighbor C-C distance of 1.425 Å was obtained in agreement with experiment.[44] The cohesive energy of a single graphene sheet was 7.85 eV and the interaction energy between two sheets 0.2 meV/C atom, displaying the well-known lack of van der Waals interactions in DFT. The interlayer distance was 3.9 Å, to be compared with the experimental 3.354 Å.

The energies of dimers were also calculated for reference (Table II). The carbon dimer is a well-known problematic case.[45] The experimental ground state being a singlet, a triplet was obtained using DFT. This was also the case using

TABLE III. Adsorption energetics of cobalt on graphite. E_{ads} is the energy as calculated by Eq. (1), $E_{ads\ vs\ hollow}$ giving this with respect to the hollow site. $d_{Co\text{-}C}$ is the shortest Co-C distance.

Site	E_{ads} (eV)	$E_{ads\ vs\ hollow}$ (eV)	$d_{Co\text{-}C}$ (Å)
Hollow	−1.12	0.0	2.10
Bridge		0.48	1.95
Top		0.56	1.88

Gaussian 03.[46] There are controversial experimental results on the binding energy of the Co_2 dimer,[47–50] whereas results on the bond length are consistent. Our DFT energy (1.46 eV) agrees with a previous result.[50] As for the CoC dimer, experimental results are also scarce.[51] Tzeli and Mavridis[32] estimated a binding energy of 1.8 eV with large differences between different levels of theory. While our result (2.5 eV) deviates from theirs significantly, the relative stabilities of the dimers are consistent. Fortunately, energies and especially energy differences in larger systems are more reliable due to cancellation of errors, but care must be taken in interpreting the results.

For calculating adsorption energetics of Co on graphite, a single graphene sheet of 60 atoms (12.825 × 12.341 Å) was used, the box size being 15.0 Å in the transverse direction to allow for sufficient space between periodic images of the system. The adsorption energy was calculated as

$$E_{ads} = E_{Co@C} - E_C - E_{Co}, \quad (1)$$

where $E_{Co@C}$ is the energy of the graphene sheet with the adsorbed atom, E_C is the energy of the clean graphene sheet, and E_{Co} is the energy of the metal atom in vacuum. The results for different adsorption sites are shown in Table III. All Co-adsorbed structures had a magnetic moment of one Bohr magneton. Cobalt was found to prefer adsorption on the sixfold coordinated hollow site of graphite.

The calculations were repeated for Co in graphite, i.e., between two graphene sheets, one farthest row of atoms in each direction being fixed at the experimental graphene sheet distance. The stable adsorption site was found with adsorption energy of −2.3 eV. The rather high value is explained by the Co atom bonding with several carbon atoms even on the top site. It is also obvious that the strength of the C-Co bonding varies according to the number of neighbors of the C atom and no single E_0 value can describe all possible configurations that can occur during an impact.

Adsorption on the hollow site is readily reproduced in MD by the Morse potential and the corresponding adsorption energy is E_{ads}=2.25 eV when the Morse parameters are E_0 =0.3 eV/atom and r_0=2.0 Å. This is two times more than the DFT value E_{ads}=1.12 eV. For an adatom between graphene sheets, MD gives E_{ads}=3.78 eV and the corresponding DFT value E_{ads}=2.3 eV is again considerably lower. The correct adsorption site is nonetheless reproduced. In both cases, the chosen Morse parameters give too strong binding between Co and C atoms. On the other hand, some Co atoms are temporarily located near a C atom during the cluster stopping phase and then the actual interaction could be more like CoC binding, which is stronger than the chosen Morse parameterization can produce. In conclusion, the chosen Morse parameters give a pinning threshold and cluster ranges that agree very well with the corresponding experimental values although the interactions at the atomistic level are correct only on average.

IV. RESULTS

A. STM study of HOPG after cluster impact

The STM study of the implanted samples shows formation of nm-size spots that are imaged as bumps. Since the virgin graphite surface is atomically smooth, their appearance can only be related to either damage introduced by the cluster impacts or by the deposited clusters themselves, depending on the impact energy regime. The surface density of the bumps correlates well with the time intervals for which different samples were exposed to the cluster beam. Thus, analysis of the surface density of bumps can be used to estimate the cluster fluence, assuming that every impact introduces one spot in the STM image. The parameters of the bumps, their shape and dimensions, are found to be dependent on the cluster impact energy. All three cluster sizes reported here demonstrate a very similar dependence of surface defect formation on the impact energy per atom. The details of the measurements are presented in Table I. As can be seen, the measured parameters are too small to rely on additional AFM study in this case.

For the energy interval of 100–200 eV/atom, one can observe the formation of bumps with mean diameters d varying between 3.0 and 4.5 nm and mean heights h of 0.35–0.45 nm (see Table I). Bumps with smaller diameters (around 3 nm) are typically imaged as hemispheres. For those with larger diameters, plateaulike disordered tops can be seen [Figs. 2(a) and 2(c)]. This difference is most probably related to the tip convolution effect which distorts the real shape of nm-size features when their lateral dimensions are comparable with the tip curvature radius. For instance, a cylindrical protrusion can be imaged as conelike or hemispherical in shape. The decrease in cluster energy does not affect significantly the height of the bumps but their diameters become smaller (Table I). Finally, for low-impact energies between 5 and 13 eV/atom for Co_{30} and Co_{50} clusters, the observed bumps have the same (within the measurement uncertainty) diameters of 1.3–1.6 nm [Table I and Fig. 2(b)]. The bumps for the case of same energy Co_{63} clusters are slightly larger.

It should also be mentioned that despite the equal deposition time (i.e., very close fluences) for Co_{50} clusters with energies 5, 7, and 9 eV/atom, the surface density of bumps is significantly lower for the 5 eV/atom case compared to the 7 eV/atom one and it is about two times lower for the 7 eV/atom deposition than for the 9 eV/atom one. Reasons for this will be discussed in Sec. V A. For further discussion of the radiation damage formation on cluster implantation, it is important to note that surface morphology for STM images is obtained from tunnel current mapping. Since the constant current mode was used for the measurements, the lift of the STM tip, producing bumps in the image, is not necessarily

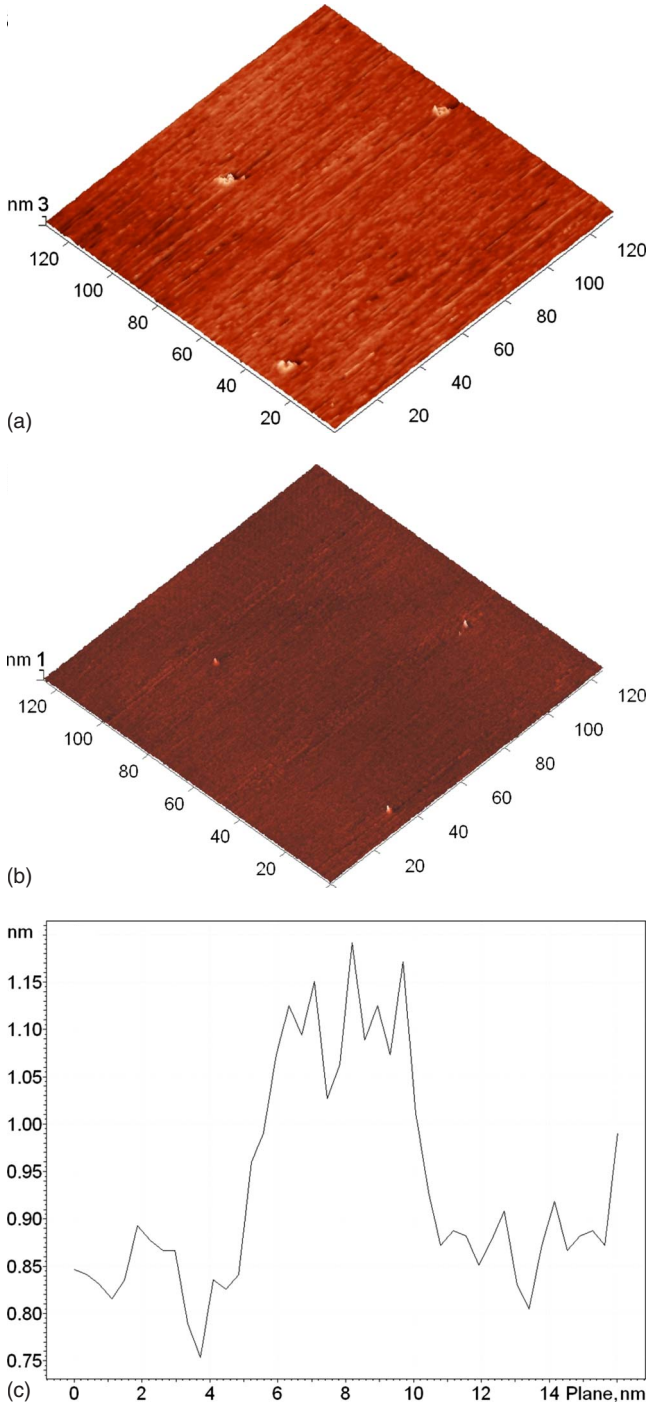

FIG. 2. (Color online) STM images of HOPG after impact of Co_{30} clusters with energies of (a) 150 and (b) 9 eV/atom. (c) Cross section of one of the bumps from image (a).

related to areal change in surface topology but can be caused by a significant change in the electronic structure of the material at the impact spots compared to the surrounding undamaged graphite. It was shown elsewhere that both vacancy and interstitial defects formed on ion implantation caused an increase in the density of states near the Fermi level.[52] The local change in electronic structure and conductance leads to a higher tunnel current that causes a lifting of the tip. Thus, the measured diameters of the bumps reflect the diameters of

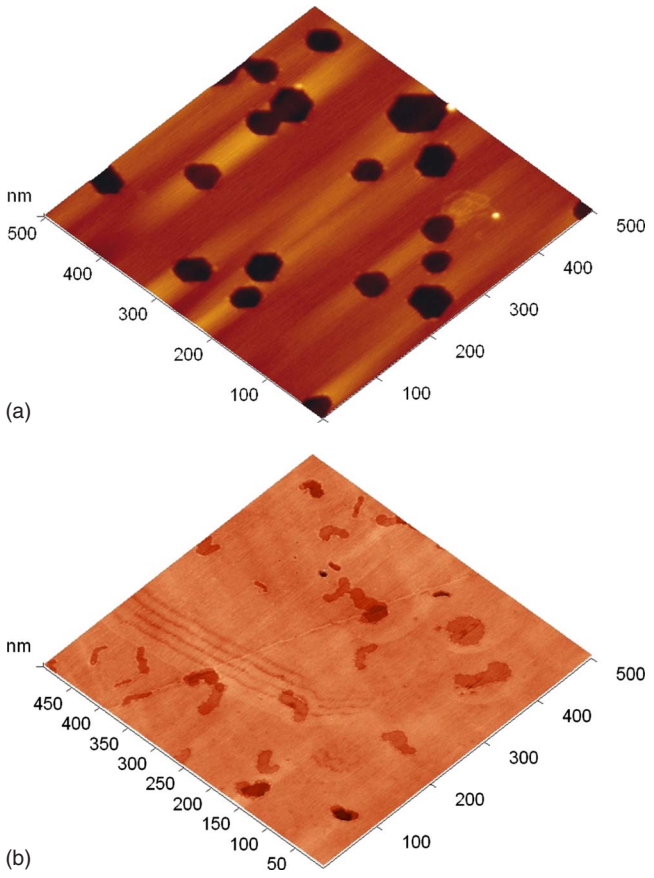

FIG. 3. (Color online) (a) AFM and (b) STM images of HOPG after impact of 130 eV/atom Co_{63} clusters and 30 eV/atom Co_{50} clusters, respectively, followed by heating at 600 °C.

the damaged areas or deposited clusters while the measured heights have a much more complex origin including both the change in topology and electronic states.

B. STM and AFM study of etched samples

It was shown elsewhere that implantation of small Ag_n and Ar_n clusters[53,54] as well as C_{60} (Ref. 25) into graphite followed by oxidative etching led to the formation of pits with depths corresponding to the introduced radiation damage. The pits had hexagonal or circular shape.

In the case of cobalt cluster impacts, we also observe the formation of pits after the heating-induced etching (Fig. 3). Their surface densities correlate well with the surface densities of bumps observed before the etching for most of the cases. The depth of the pits is found to be an increasing function of the cluster energy. This dependence is presented in Fig. 4 and it will be discussed in Sec. V B. However, only the deepest pits originated by the implantations with the highest energies (150–200 eV/atom) have hexagonal shape [Fig. 3(a)]. For the case of moderate implantation energies (50–100 eV/atom), one can observe the appearance of wormlike channels [Fig. 3(b)], which become the dominant structures for the samples implanted with energies of 9–30 eV/atom. This tendency of transition from hexagonal pits to wormlike channels with a decrease in cluster impact energy

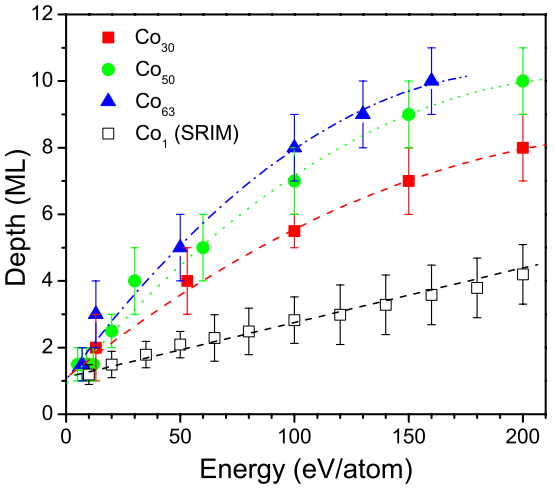

FIG. 4. (Color online) Experimentally found dependence of depth of etched pits on cluster size and impact energy. Symbols with uncertainties represent experimental data while dashed and dotted lines show fitting with function $E_{at}^{1/2}$. Simulated by SRIM-2008 dependence of Co monomer R_p on implantation energy is also presented. Uncertainties show calculated R_p straggling.

is found to be very similar for all cluster sizes investigated in this study. The depth of the channels depends on the impact energy. Their width is typically between 5 and 15 nm. Quite often they have one end slightly wider than the other one. The length of the channels increases with a decrease in cluster energy reaching 200–300 nm in some cases. It should be noted that both STM and AFM observations demonstrate very similar channels except that there is always a few nm high bump at the narrow end of every channel on AFM images while there are no such protrusions observed by STM, as one can see in Fig. 5. For cluster energies below 9 eV/atom and sizes $n=30$ and 50, the surface density of the etched areas becomes vanishingly small, at least significantly lower than the surface density of bumps observed before the etching.

C. MD simulations of Co_n cluster impact

At low energies ($E=1-10$ eV/atom), cluster atoms form a monolayer island on the surface in the simulations [Figs. 6 and 7]. The graphite structure reacts elastically upon impact and no damaged region is formed. During the impact, the cluster falls apart due to the attractive interaction between Co atoms and surface C atoms. In a relaxed system, most Co atoms in the islands are located at the surface and in the middle of C rings. The diameter of the Co islands, which is about 1.5 nm, is in agreement with experimental results for low-impact energies (5–13 eV/atom). The flatness of experimentally observed islands ($h<3.5$ Å) indicates that the cluster is also transformed in reality. If the Co-C equilibrium distance in the potential is changed to correspond to that of CoC(1.5 Å), Co atoms penetrate through the layers and no island is formed. Also weakening of the attractive C-Co interaction decreases island formation.

The form of the islands is irregular and some single add atoms are detected in the surrounding area. Surface diffusion

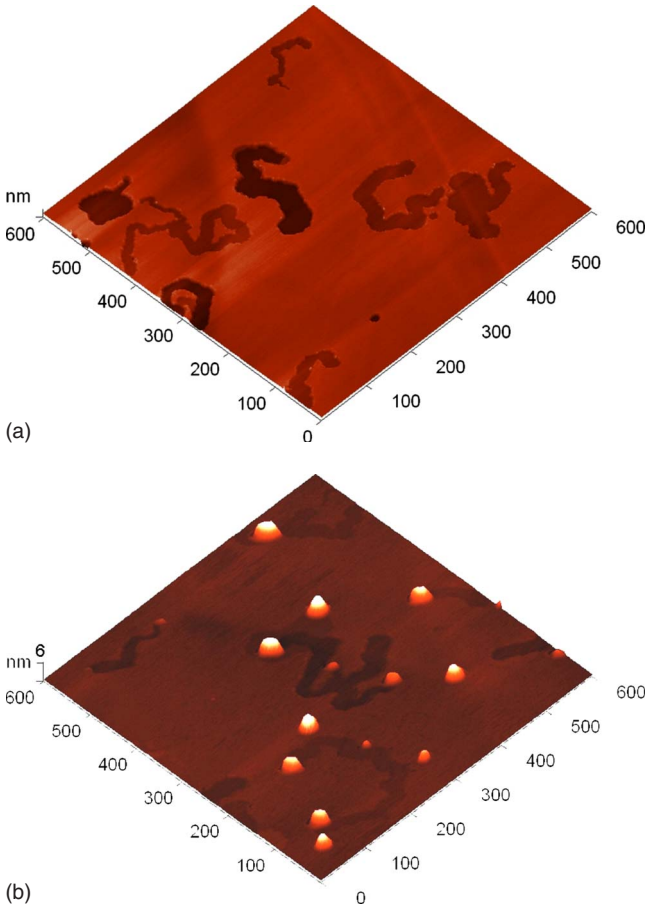

FIG. 5. (Color online) Surfaces of HOPG after impact of 13 eV/atom Co_{50} clusters followed by heating at 600 °C imaged by (a) STM and (b) AFM, respectively.

of Co atoms is not simulated but the effects of diffusion can be deduced. First, the Co-Co interaction decreases the probability that the island atoms would diffuse away from the island. Second, single Co add-atoms that diffuse close to an island join the island. The result is a group of solid islands on the surface. However, an island may also disappear due to diffusion if it is initially very sparse. At 10–20 eV/atom, some Co atoms penetrate through the first graphite layer. This probably "locks" the islands more tightly onto the surface and diffusion cannot destroy them as easily as for islands without these locking atoms.

When the impact energy increases, the Co atoms start to penetrate deeper through the graphite layers and a crater-shaped damaged region is formed (Fig. 6). It consists of Co and C atoms arranged almost randomly, although the layer structure is still partially present. Similar results are reported also in other MD studies.[55,56] At energies higher than 50 eV/atom, all Co atoms travel through the first graphite layers and stop in the inner parts of the graphite. This transition from shallow to deep implantation occurs gradually. At these impact energies and cluster sizes, the damaged region does not considerably expand after the stopping of Co atoms. In dense substrates, e.g., Si and Au, the stopping phase induces a high-energy region where the primary collisions have occurred. This energy induces an expansion of the damaged

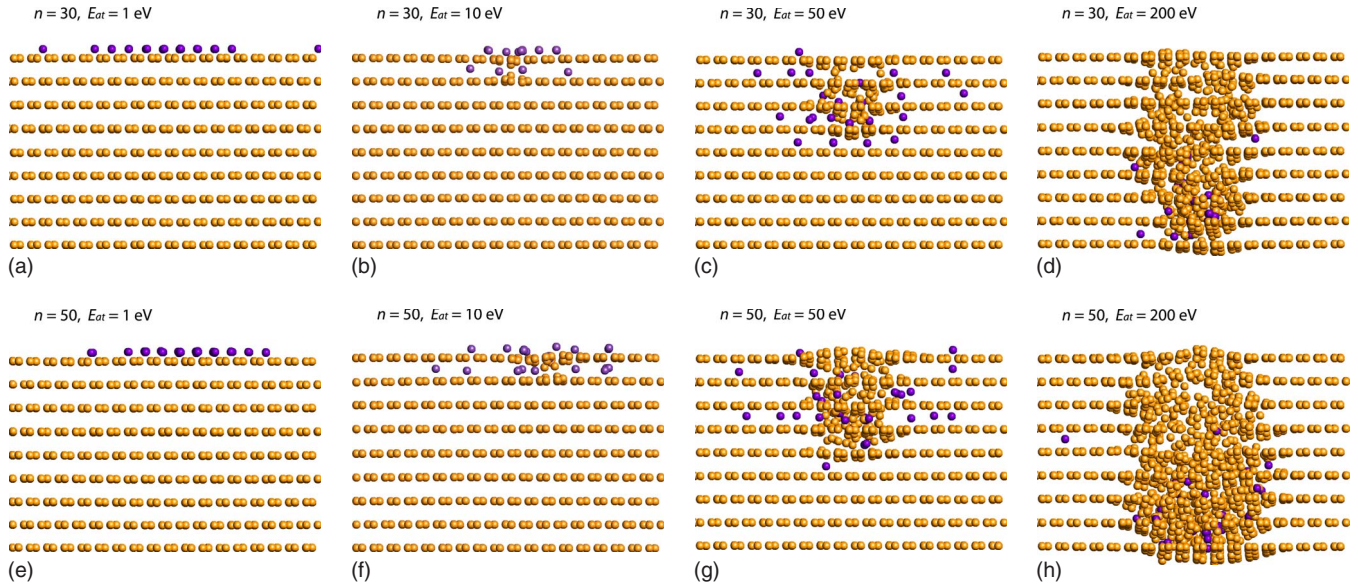

FIG. 6. (Color online) Examples of simulated damage created at 1, 10, 50, and 200 eV/atom by Co_{30} (top) and Co_{50} (bottom) clusters. Width of each frame is 4 nm. Co atoms are shown in the darker shade.

region, which leads to formation of craters larger than the original cluster track.[5] In the present simulations, damage is created mostly by the collisions between Co and C atoms. Thus, the geometry of the damaged region is a consequence of collision dynamics at the cluster stopping phase, which is the reason for the scaling of damage depth with cluster momentum, as will be discussed in Sec. V B. In addition, the absence of a high-temperature core leads also to a low-sputtering yield, in particular, the Co atoms are seldom sputtered. The width of the damaged region is 1–3 nm and it is not much wider than the diameter of the cluster. Because of the rather short simulation time typical for MD simulations, it is not possible to see, whether or not the top layers are healed and the damage is contained inside the substrate.

The Co atoms that have gained lateral momentum in the collisions, travel away from the damaged region between graphite layers and stop at a distance of 1–2 nm. The core damaged region is thus surrounded by a 3–4 nm wide region of Co interstitials. In the time-scale typical for MD, it is not possible to simulate whether or not these interstitials diffuse away from the impact area or join to the damaged area. If they diffuse away, the final number of Co atoms below the impact point is considerably smaller than the initial number of Co atoms in the cluster. The width of the interstitial region decreases with increasing energy because the scattering angle of Co atoms decreases with increasing momentum and it becomes less probable that Co atoms scatter to interlayer spaces.

V. DISCUSSION

A. Implantation and pinning of clusters

It was shown in earlier MD studies that the formation of craters on graphite is a quite probable scenario for high-energy impact of a cluster at least at its initial stage: for instance, for 5.5 keV Ag_{147} clusters[55] and 100 eV/atom Au_n ($n=13-402$) clusters.[57] The clusters were shown to be broken and the constituents came to rest inside a damaged region. However, due to the very elastic response of the graphite planes to the impact, only a small region of the lattice was damaged and craters were small. Moreover, the craters can partly or fully recover at a later stage because of the relaxation of the graphite layers. This effect is especially essential

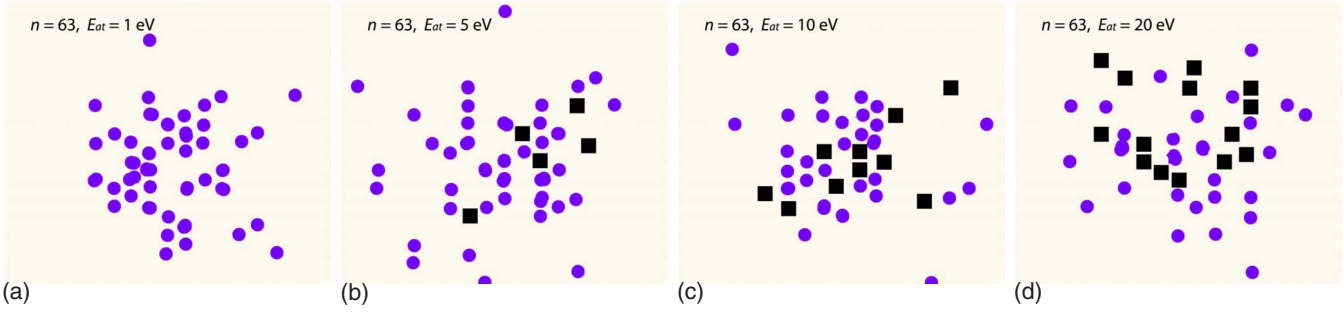

FIG. 7. (Color online) Examples of simulated Co islands on graphite surface at impact energies of 1, 5, 10, and 20 eV/atom (Co_{63}). Dark squares show positions where Co atoms are implanted just below the first graphite layer. All 63 Co atoms are not shown because some atoms are piled and not visible in this perspective. A few atoms are also sputtered. Width of each frame is 4 nm.

for the case of small clusters even if the implantation energy is relatively high, for example for 555 eV/atom Ta_n ($n=4,9$), 500 eV/atom Ar_{12}, and 100 eV/atom Au_{13} clusters.[57–59]

Our current MD simulations also show that no clear craters are formed. Instead, there is an amorphous region that contains Co atoms and small voids (Fig. 6). The top of the damaged region can form a small bump. Thus, the very similar surface features observed by STM for the 100–200 eV/atom cluster implantations most probably represent partly recovered impact regions where C atoms are intermixed with implanted cobalt. Despite the breakage of the cluster upon impact, most of the atoms come to rest close to each other at the final stage of impact as shown by the simulations. Hence, one can conclude that there is a residual cluster at the bottom of the collision cascade. Taking into account the possible tip convolution effect, the simulated diameters of damaged areas of 2–3 nm for the above-mentioned energy interval are in good agreement with experimentally measured diameters of bumps, 3.5–4.5 nm.

It is obvious that a decrease in cluster kinetic energy leads to a decrease in cluster implantation depth (or projected range of cluster constituents) and to smaller radiation damaged volumes. According to the MD simulations such a transition to "shallow" implantation, where the residual cobalt is located just beneath the surface, can occur at energies below 50 eV/atom for the cluster sizes studied here. In the STM images this transition is reflected by a decrease in the diameter of the bumps from approximately 3.5 nm at 100 eV/atom to approximately 2.5 nm at 20–60 eV/atom. This small decrease in lateral dimensions of the damaged areas is also in good agreement with the simulations (Figs. 6).

It was shown elsewhere[12] that further decrease in cluster kinetic energy leads to a transition from the implantation to the so-called pinning regime where, on the one hand, the impact energy is still high enough to displace one or a few C atoms from their sites in the top graphite layer but, on the other hand, the kinetic energy per atom is of the same order as the binding energy of atoms in the cluster and, thus, the cluster can be preserved as a whole. In this way, a defect on the surface is created to which the cluster becomes bound. Hence, transition to the pinning regime allows the deposition of size-selected clusters and prevents their subsequent diffusion on the surface. This is of utmost importance for practical applications. The pinning threshold energy was found to be a function of cluster species, size, structure, and type of substrate material.[13,14] Using MD simulations in comparison with experimental results, a semiempirical model of how the pinning threshold energy depends on cluster and substrate parameters was developed and tested for Ag_n, Au_n, Ni_n, and Pd_n clusters deposited on graphite.[12–14,56] According to this model, the pinning energy is given by

$$E_{\mathrm{pin}} = nm_{\mathrm{cl}}\frac{E_T}{4m_{\mathrm{sub}}}, \tag{2}$$

where n is the cluster size, m_{cl} and m_{sub} are the atomic masses of the chemical elements forming the cluster and the substrate, respectively, and E_T is the energy transferred to an atom of the substrate to displace it from a lattice site. E_T can also be interpreted as the energy required to produce a vacancy or interstitial defect. The reported values for vacancy and interstitial formation in graphite vary between 5.5–7.0 eV.[56] By putting these values into Eq. (2) one can predict the "pinning threshold window" for Co_n clusters on graphite to be between approximately 7–9 eV/atom. However, the model assumes that only one C atom is set in motion by the cluster. If the cluster displaces all C atoms in the layer under the cluster then a new parameter, the number of displaced atoms, must be added to the denominator. This makes the pinning energy size dependent. We might therefore expect a dependence of E_{pin} somewhere between two boundary cases $\approx n$ and $\approx n^{1/3}$.[56]

Our MD simulations predict the transition from shallow implantation to pinning (some Co atoms penetrate through the top graphite layer) at an energy of around 10 eV/atom for Co_{30} and Co_{50} clusters. Since these sizes do not differ by much, there is no significant difference observed for the pinning energy. This value is in reasonable agreement with those predicted by the model. Our MD simulations show that small clusters have a tendency to be flattened to monolayers with a few atoms embedded between the first and second graphite planes (Figs. 6 and 7). The diffusion of the Co atoms is prevented by the rather strong Co-Co interaction. The simulated flattened clusters (islands) have lateral dimensions up to 1.5 nm. The STM data give diameters of bumps, formed on impact of cobalt clusters with energies between 5 and 13 eV/atom, of 1.3–1.6 nm, except for 13 eV/atom Co_{63}, where $d=2.6$ nm (see Table I). Thus, taking into account the predicted "pinning window" and the MD simulations for low-energy cluster impacts we can suggest that the bumps observed in the STM images after cluster impact at energies ≤ 13 eV/atom most probably correspond to the pinned and flattened clusters.

It was mentioned in Sec. IV A that the surface density of bumps formed after the deposition of Co_{50} clusters decreases with cluster energy (for the interval of 9–5 eV/atom) despite the same deposition time (fluence). It is likely that decrease in the energy from 9 to 5 eV/atom leads to only a fraction of the clusters becoming pinned, i.e., immobilized on the surface, making their detection possible. The rest do not create stable bonding sites with carbon hexagons. These clusters can diffuse to surface defects, for instance, to graphite steps where they become unresolved by STM. Since the clusters are flattened to monolayers and irregular in shape, we can also suppose that some Co atoms, which are not bound to graphite, can leave the sparse islands thus providing an additional channel for the disappearance of the clusters. These suggestions can explain the decrease in surface density of bumps for the lowest deposition energies investigated. Further proof of the validity of our model describing the transition from "deep" to "shallow" implantation and then to pinning is obtained from the etching experiments.

B. Stopping of cluster constituents in graphite: scaling law

Figure 4 shows the experimentally obtained dependence of the depth of etched pits (in number of graphite layers) on impact energy per atom E_{at}. The kinetic energies were in the

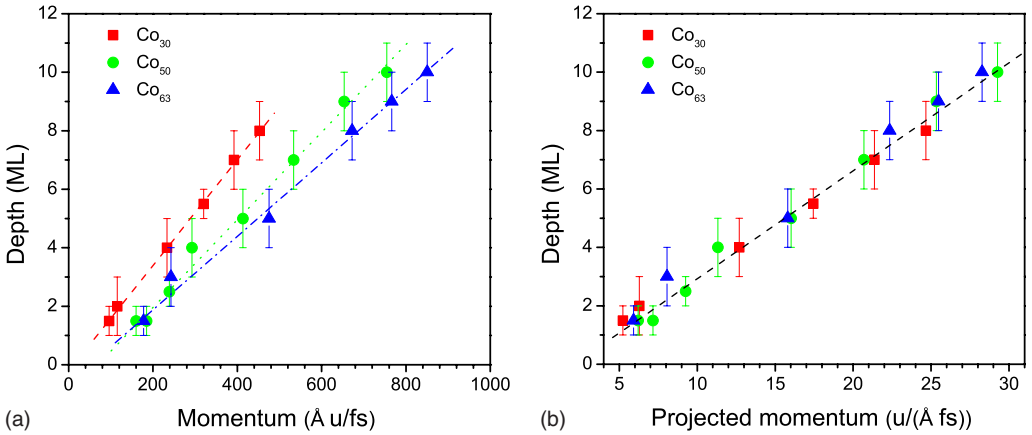

FIG. 8. (Color online) Experimentally found dependence of depth of etched pits on (a) ordinary and (b) projected cluster momentum for different cluster sizes. Symbols with uncertainties represent experimental data while dashed and dotted lines show fitting with function $a_n + b_n p$. See text for details.

range between 5 and 200 eV/atom, which can be considered as a very low-energy implantation regime. For such low energies, the radiation damage produced in graphite is not very much wider and deeper than the primary stopping region of Co atoms, which is a consequence of the very elastic response of the graphite lattice to the cluster impact, as already mentioned in the previous section. Thus, the experimentally measured depth corresponds to the depth of radiation damage caused by the implanted cluster constituents and should be very close to the projected range R_p of the deepest Co atoms. In the same figure one can also see a dependence of mean R_p vs E_{at} for Co monomers implanted into amorphous carbon which is calculated using the SRIM-2008 code.[30] The density of amorphous C is chosen to be equal to that of graphite to relate the simulation to the experimental case. One can see that for the case of monomers the dependence is a linear function of energy while for the clusters the depth can be approximated with very good precision by the $E_{\mathrm{at}}^{1/2}$ function for all cluster sizes. In Fig. 4 one can see that the projected ranges of cluster constituents are higher compared to monomers, as well as that larger clusters are implanted deeper than smaller ones at the same E_{at}.

The observed square root dependence of R_p on E_{at} leads to the suggestion that the projected range can be represented as a linear function of cluster momentum. The dependence in these coordinates is presented in Fig. 8(a) and it follows the relation

$$R_p = a_n + b_n p_{\mathrm{cluster}} = a_n + b_n M v_{\mathrm{cluster}}, \qquad (3)$$

where a_n and b_n are the cluster-size-dependent variables and p_{cluster}, M, and v_{cluster} are the cluster momentum, mass, and velocity, respectively. The linear dependence of the cluster implantation depth in graphite on the cluster momentum was earlier reported for Au_7 and Ag_7 clusters and for a series of small (from 3 to 13 atoms) silver clusters.[53,60] The observation of a linear dependence on momentum is consistent with a braking force, which is proportional to the normal velocity of the cluster, akin to Stokes' law.[60] Our experimental data support this cluster stopping model and extend it to another cluster species as well as to larger cluster sizes.

Following the arguments given by Seminara *et al.*,[53] we divide the momentum of an n-atom cluster by $n^{2/3} r_{WS}^2$, where r_{WS} is the Wigner-Seitz or Voronoi radius of cobalt. In other words, we scale the momentum with the projected surface area of the cluster, assuming the spherical approximation. The results are shown in Fig. 8(b) and it is clearly seen that the data points now all fit very well onto a single straight line. This provides very strong support for the assertion made in Ref. 53 that the cluster implantation depth is a linear function of momentum per unit surface area. The generality of this statement can now be clearly seen in Fig. 9 where we plot the straight line fit from Fig. 8(b) together with the implantation data taken from the literature for Si_7, Au_7, and Ag_n for $n=7$ and 13.[53,60] For this comparison we have used the cluster projected surface area for the silver clusters, calculated with DFT, as used by Seminara *et al.*[53] and have considered the same geometry for Au_7 as for Ag_7. The projected surface area for Si_7 was scaled from Au_7, assuming the same

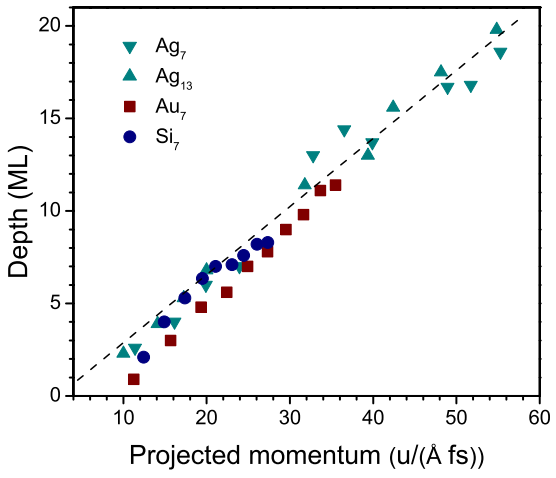

FIG. 9. (Color online) Comparison of the straight line fit [same as in Fig. 8(b)] for depth of radiation damage introduced by implanted Co_n clusters with experimental data from the literature. Au_7 (squares) and Si_7 (circles) from Ref. 60, Ag_7 (down-triangles) and Ag_{13} (up-triangles) from Ref. 53. All implantations were carried out in HOPG.

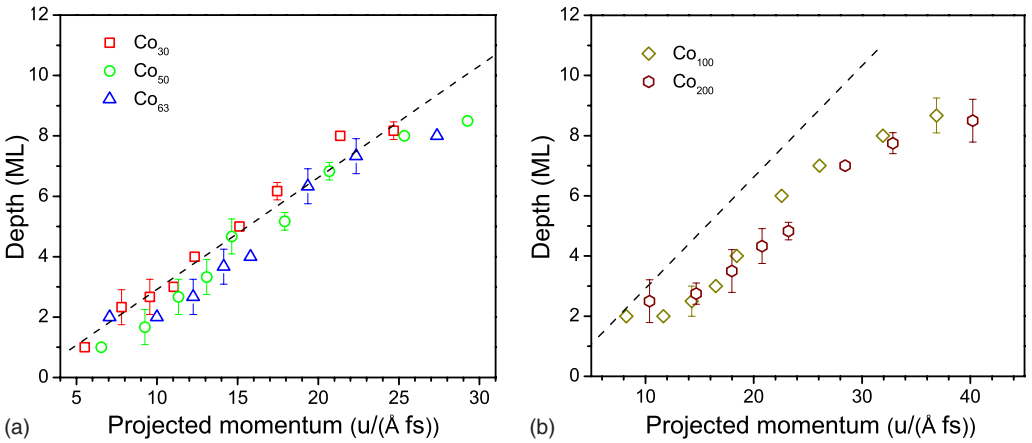

FIG. 10. (Color online) Simulated dependences of depth of deepest implanted Co atoms on projected momentum for different cluster sizes: (a) Co_{30}, Co_{50}, and Co_{63}, and (b) Co_{100} and Co_{200}. The fitting of experimentally obtained dependences [same as in Fig. 8(b)] is presented for comparison by dashed line.

geometrical structure[61] but scaling the projected cross section by the square of the ratio of bond lengths for Au-Au and Si-Si (approximately 1.5 smaller for Si_7). The same universal plot is obtained, regardless of the cluster constituent.

The other conclusion that can be made from the dependencies presented in Fig. 4 is that at implantation energies ≤ 13 eV/atom the penetration depth of the cluster constituents is 1–2 ML, consistent with the pinning threshold energy of 10 eV/atom obtained from the MD simulations. An exception is the case of 13 eV/atom Co_{63} clusters for which the depth of etched pits is found to be 3 ± 1 ML. In terms of momentum this case is very close to one representing implantation of Co_{50} with an energy of 20 eV/atom, corresponding to shallow implantation and yielding a depth of 2–3 ML. Thus, the projected momentum scaling provides a convenient estimate of the expected pinning threshold energy.

The average maximum depth of implanted Co atoms extracted from the MD simulations and presented in Fig. 10(a) also shows the same dependence on cluster momentum. The calculated values of R_p for Co_{30}, Co_{50}, and Co_{63} clusters are in good agreement with those found experimentally at energies comparable to the experimental impact energies. However, at larger cluster sizes or higher energies (higher cluster momenta) the scaling becomes different: the simulations show a weaker dependence on cluster size [Fig. 10(b)]. A probable reason for this is the piling-up of atoms at the front of the cluster because not all C atoms can escape the cluster or fit between the cluster atoms if the cluster is large enough. A high-density region is formed and this resists the movement of the cluster. Such a phenomenon has recently been demonstrated for large Au clusters.[9,62]

C. Selective etching of graphite surface

One more phenomenon found after the heating-induced etching should be addressed in this paper: the transition from hexagonal shaped pits to wormlike channels with decreasing cluster impact energy. For moderate and low energies the implantation becomes shallow, the projected range of cluster constituents is a few ML and as shown by the MD simulations (Fig. 6), the cluster atoms are located very close to each other in the damaged area. One can assume that Co-Co bonds are restored to some extent, in other words, there is a residual cluster located in the shallow graphite layer. High temperature increases the diffusive mobility of these residual clusters and at the same time they catalyze the reaction of atmospheric oxygen with carbon, thus, favoring the formation of planar surface channels of random shape. Similar effects were reported elsewhere on the deposition of various chemical substances on graphite surfaces followed by heating-induced etching.[23] The same phenomenon was recently reported for Fe nanoparticles deposited on few-layer graphene.[17] While exposed to 900 °C, the nanoparticles etched away the graphene sheets producing channels. Trench channeling of graphene was also demonstrated by silver nanoparticles under heating up to 650 °C in ambient atmosphere.[63]

Molecular dynamics simulation of the graphite with an embedded cluster is not able to predict diffusion of the residual cluster. However, one can see in MD that the heating leads to partial separation from the substrate of a few top planes of graphite which are probably locked to each other by the embedded cobalt atoms. This type of separation can promote a more effective start for the etching.

In our case the depth of etched channels and their length can be controlled through the impact energy. At lower energies the cluster penetrates less and it is less fragmented. Therefore, its catalytic activity is higher and the channels become longer. At impact energies below 9 eV/atoms and sizes $n=30$ and 50 the surface density of channels is significantly lower compared to the density of Co islands before the heating. This leads us to the conclusion that a considerable number of the clusters deposited with these energies are bound to the graphite surface very weakly producing almost no defects in the top plane. On heating, these Co agglomerates do not cause etching but diffuse away or possibly become sublimed.

Comparison of the STM and AFM images presented in Fig. 5 allows some conclusions to be formed about the products of the catalytically activated etching. It is well known

that the reaction between carbon and oxygen typically causes formation of volatile gases CO and CO_2. However, the presence of the bumps at the narrow end of the channels leads us to the conclusion that some of the etched carbon is collected around the moving cluster. The fact that these bumps are not observed in the STM images is evidence that the bumps have lower conductance compared to the surrounding graphite. Clarification of the nature of these bumps requires special study.

VI. CONCLUSIONS

We have studied the interaction of energetic size-selected Co_n clusters with HOPG both experimentally and theoretically. The results of the experimental STM and AFM studies on the HOPG after the cluster implantation and deposition are in good agreement with the MD simulations. It is found that energetic cluster impact leads to the formation of nm-size damaged areas; with decrease in cluster kinetic energy there is a transition from "deep" to "shallow" implantation and then further to so-called cluster pinning. For "deep" implantation, the impacting cluster creates considerable damage in the target. At the beginning of the collision, there is the possibility of opening a small crater which recovers at a later stage. For "shallow" implantation, there is the formation of a shallow disordered region where Co atoms are intermixed with C ones. For cluster energies around 10 eV/atom evidence is seen for the transition to pinning, i.e., the impacting cluster produces a small damaged site in the top graphite layer and becomes relatively strongly bound to it (immobilized). However, it is found that the pinned cobalt clusters are flattened; they prefer to form monolayer islands if they are not large (few tens of atoms in size). A further decrease in the cluster energy leads to weakening of bonds between the deposited clusters and surface that in turn leads to lower stability and easier surface diffusion of the clusters.

Etching of the radiation damaged areas introduced by cluster impacts provided a measure of the depth to which the collision cascades are developed and allowed a comparison of these data with the MD simulations. Very good quantitative agreement was found. It was concluded that the projected range of the cluster constituents could be scaled as the square root of their energy. Larger clusters introduce deeper radiation damage compared to the smaller ones if the energy per atom of the cluster is the same. Thus, convincing evidence for the simple mechanical nature of the cluster stopping and damage formation in graphite is presented both experimentally and theoretically.

We have shown that a plot of the implantation depth versus projected momentum produces a universal straight line behavior, illustrated by plotting the straight line fit to the Co_n data together with implantation data on cluster impact for Si_n, Au_n, and Ag_n clusters available in the literature. The same behavior is well reproduced by the MD simulations for Co_n cluster impact with $n=30$, 50 and 63 but is seen to deviate for higher cluster masses probably due to formation of a high-density region at the front of the moving cluster.

The formation of surface channels (trenches) after the heating-induced etching of graphite is of considerable interest both from fundamental and application-oriented points of view. It shows that even after quite energetic impacts there are residual clusters which remain intact in the shallow graphite layer. Higher temperature increases the diffusive mobility of these clusters and the presence of active gases can ignite catalytic reactions. In particular, in the presence of oxygen it leads to the etching of narrow trenches in the top few graphene layers. Thus, small imbedded Co nanoparticles can be used as a processing tool for graphene. However, more extensive study of this catalytic phenomenon is required.

ACKNOWLEDGMENTS

We would like to thank Arkadi Krasheninnikov for valuable discussions. Three of the authors (V.N.P., S.V., and E.E.B.C.) are grateful for the financial support of the Swedish Research Council and Knut and Alice Wallenberg Foundation. The computational part of this work was performed within the Finnish Centre of Excellence in Computational Molecular Science (CMS), financed by The Academy of Finland and the University of Helsinki.

*popok@physics.gu.se

[1] P. Jena and A. W. Castleman, Proc. Natl. Acad. Sci. U.S.A. **103**, 10560 (2006).
[2] K. Wegner, P. Piseri, H. V. Tafreshi, and P. Milani, J. Phys. D **39**, R439 (2006).
[3] V. N. Popok and E. E. B. Campbell, Rev. Adv. Mater. Sci. **11**, 19 (2006).
[4] N. Toyoda and I. Yamada, IEEE Trans. Plasma Sci. **36**, 1471 (2008).
[5] J. Samela and K. Nordlund, New J. Phys. **10**, 023013 (2008).
[6] J. Borland, J. Hautala, M. Gwinn, T. Tetreault, and W. Skinner, Solid State Technol. **47**, 53 (2004).
[7] J. Gspann, in *Large Clusters of Atoms and Molecules*, edited by T. P. Martin (Kluwer, Amsterdam, 1996), p. 443.
[8] V. Popok, S. Prasalovich, and E. Campbell, Vacuum **76**, 265 (2004).
[9] J. Samela and K. Nordlund, Phys. Rev. Lett. **101**, 027601 (2008).
[10] V. Popok, in *Handbook of Nanophysics*, Vol. 2, edited by K. D. Sattler (CRC Press, Boca Raton, in press).
[11] P. Jensen, Rev. Mod. Phys. **71**, 1695 (1999).
[12] S. J. Carroll, S. Pratentep, M. Streun, R. E. Palmer, and R. Smith, J. Chem. Phys. **113**, 7723 (2000).
[13] M. Di Vece, S. Palomba, and R. E. Palmer, Phys. Rev. B **72**, 073407 (2005).
[14] S. Gibilisco, M. D. Vece, S. Palomba, G. Faraci, and R. E. Palmer, J. Chem. Phys. **125**, 084704 (2006).
[15] S. Serrano-Guisan, G. di Domenicantonio, M. Abid, J.-P. Abid,

M. Hillenkamp, L. Gravier, J.-P. Ansermet, and C. Félix, Nature Mater. **5**, 730 (2006).
[16] S. Noda, Y. Tsuji, Y. Murakami, and S. Murayama, Appl. Phys. Lett. **86**, 173106 (2005).
[17] S. S. Datta, D. R. Strachan, S. M. Khamis, and A. T. C. Johnson, Nano Lett. **8**, 1912 (2008).
[18] K. Nordlund, Comput. Mater. Sci. **3**, 448 (1995).
[19] S. Vučković, M. Svanqvist, and V. N. Popok, Rev. Sci. Instrum. **79**, 073303 (2008).
[20] V. N. Popok, S. V. Prasalovich, M. Samuelsson, and E. E. B. Campbell, Rev. Sci. Instrum. **73**, 4283 (2002).
[21] V. Popok, S. Prasalovich, and E. Campbell, Nucl. Instrum. Methods Phys. Res. B **207**, 145 (2003).
[22] S. Vučković, J. Samela, K. Nordlund, and V. N. Popok, Eur. Phys. J. D **52**, 107 (2009).
[23] H. Chang and A. Bard, J. Am. Chem. Soc. **113**, 558 (1991).
[24] F. Stevens, L. Kolodny, and T. Beebe, J. Phys. Chem. B **102**, 10799 (1998).
[25] G. Bräuchle, S. Richard-Schneider, D. Illig, R. D. Beck, H. Schreiber, and M. M. Kappes, Nucl. Instrum. Methods Phys. Res. B **112**, 105 (1996).
[26] K. Nordlund, M. Ghaly, R. S. Averback, M. Caturla, T. Diaz de la Rubia, and J. Tarus, Phys. Rev. B **57**, 7556 (1998).
[27] M. Ghaly, K. Nordlund, and R. S. Averback, Philos. Mag. A **79**, 795 (1999).
[28] K. W. Jacobsen, J. K. Norskov, and M. J. Puska, Phys. Rev. B **35**, 7423 (1987).
[29] K. Nordlund, J. Keinonen, and T. Mattila, Phys. Rev. Lett. **77**, 699 (1996).
[30] J. F. Ziegler, J. P. Biersack, M. D. Ziegler, *The Stopping and Ranges of Ions in Matter* (Lulu Press, Morrisville, 2008).
[31] L. Sandoval and H. M. Urbassek, Phys. Rev. B **79**, 144115 (2009).
[32] D. Tzeli and A. Mavridis, J. Phys. Chem. A **110**, 8952 (2006).
[33] A. Follett, K. A. McNabb, A. A. Peterson, J. D. Scanlon, C. J. Cramer, and K. McNeill, Inorg. Chem. **46**, 1645 (2007).
[34] J. Lahtinen, K. Kauraala, J. Vaari, T. Vaara, P. Kaukasoina, and M. Lindroos, Phys. Rev. B **63**, 155402 (2001).
[35] J. C. W. Swart, I. M. Ciobíca, R. A. van Santen, and E. van Steen, J. Phys. Chem. C **112**, 12899 (2008).
[36] G. Kresse and J. Hafner, Phys. Rev. B **47**, 558 (1993).
[37] G. Kresse and J. Hafner, Phys. Rev. B **49**, 14251 (1994).
[38] G. Kresse and J. Furthmüller, Phys. Rev. B **54**, 11169 (1996).
[39] G. Kresse and J. Furthmüller, Comput. Mater. Sci. **6**, 15 (1996).
[40] P. E. Blöchl, Phys. Rev. B **50**, 17953 (1994).
[41] G. Kresse and D. Joubert, Phys. Rev. B **59**, 1758 (1999).
[42] J. P. Perdew, K. Burke, and M. Ernzerhof, Phys. Rev. Lett. **77**, 3865 (1996).
[43] P. E. Blöchl, O. Jepsen, and O. K. Andersen, Phys. Rev. B **49**, 16223 (1994).
[44] *Handbook of Chemistry and Physics: Internet Version*, 88th ed. (Taylor & Francis, London, 2007).
[45] M. R. Pederson and K. A. Jackson, Phys. Rev. B **43**, 7312 (1991).
[46] M. J. Frisch *et al.*, Tech. Rep. Gaussian 03, Revision C.02, Gaussian, Inc. (2004).
[47] A. Kant and B. Strauss, J. Chem. Phys. **41**, 3806 (1964).
[48] C. Jamorski, A. Martinez, M. Castro, and D. R. Salahub, Phys. Rev. B **55**, 10905 (1997).
[49] D. A. Hales, C.-X. Su, L. Lian, and P. B. Armentrout, J. Chem. Phys. **100**, 1049 (1994).
[50] S. Datta, M. Kabir, S. Ganguly, B. Sanyal, T. Saha-Dasgupta, and A. Mookerjee, Phys. Rev. B **76**, 014429 (2007).
[51] A. G. Adam and J. R. D. Peers, J. Mol. Spectrosc. **181**, 24 (1997).
[52] J. R. Hahn and H. Kang, Phys. Rev. B **60**, 6007 (1999).
[53] L. Seminara, P. Convers, R. Monot, and W. Harbich, Eur. Phys. J. D **29**, 49 (2004).
[54] HOPG was implanted by 17 keV $Ar_{41\pm2}$ clusters. Heating of the sample at 600 °C for 3 min in ambient atmosphere leads to the formation of hexagonal in shape pits with depth of 2.7 ± 0.7 nm (8 ± 2 ML) as found by STM measurements.
[55] S. J. Carroll, P. D. Nellist, R. E. Palmer, S. Hobday, and R. Smith, Phys. Rev. Lett. **84**, 2654 (2000).
[56] R. Smith, C. Nock, S. D. Kenny, J. J. Belbruno, M. Di Vece, S. Palomba, and R. E. Palmer, Phys. Rev. B **73**, 125429 (2006).
[57] C. Anders and H. M. Urbassek, Nucl. Instrum. Methods Phys. Res. B **228**, 57 (2005).
[58] M. Henkel and H. M. Urbassek, Nucl. Instrum. Methods Phys. Res. B **145**, 503 (1998).
[59] J. Samela, K. Nordlund, J. Keinonen, V. Popok, and E. Campbell, Eur. Phys. J. D **43**, 181 (2007).
[60] S. Pratontep, P. Preece, C. Xirouchaki, R. E. Palmer, C. F. Sanz-Navarro, S. D. Kenny, and R. Smith, Phys. Rev. Lett. **90**, 055503 (2003).
[61] S. Li, R. J. V. Zee, W. Weltner, and K. Raghavachari, Chem. Phys. Lett. **243**, 275 (1995).
[62] J. Samela and K. Nordlund, Nucl. Instrum. Methods Phys. Res. B **267**, 2980 (2009).
[63] N. Severin, S. Kirstein, I. M. Sokolov, and J. P. Rabe, Nano Lett. **9**, 457 (2009).